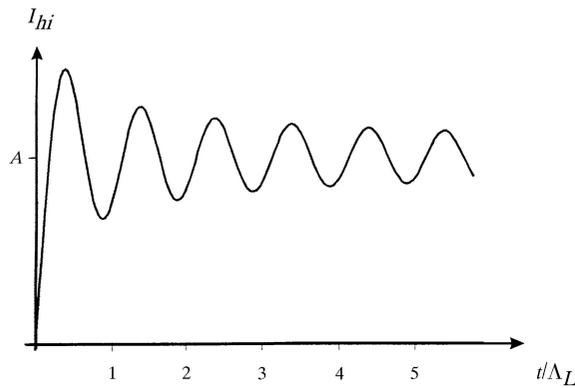## 5.1. DYNAMICAL THEORY OF X-RAY DIFFRACTION

Fig. 5.1.6.7. Variations with crystal thickness of the integrated intensity in the transmission case (no absorption) (arbitrary units). The expression for A is given in the text.

$$A = \frac{R\lambda^2 |CF_h|(\gamma)^{1/2}}{2V \sin 2\theta}.$$

Fig. 5.1.6.7 shows the variations of the integrated intensity with t/Λ_L.

5.1.6.5.2. *Absorbing crystals*

The integration was performed for absorbing crystals by Kato (1955). The integrated intensity in this case is given by

$$I_{hi} = A|F_h/F_{\bar{h}}| \exp\left[-1/2\mu_o t(\gamma_o^{-1} + \gamma_h^{-1})\right]$$
$$\times \left[\int_0^{2\pi t\Lambda_L^{-1}} J_0(z)\, \mathrm{d}z - 1 + I_0(\zeta)\right],$$

where

$$\zeta = \mu_o t \left\{\left[|C|^2 |F_{ih}/F_{io}|^2 \cos^2\varphi + (\gamma_h - \gamma_o)/(4\gamma_o\gamma_h)\right]/(\gamma_o\gamma_h)\right\}^{1/2}$$

and $I_0(\zeta)$ is a modified Bessel function of zeroth order.

5.1.6.6. *Thin crystals – comparison with geometrical theory*

Using (5.1.6.6) and (5.1.6.7), the reflecting power of the reflected beam may also be written

$$I_h = \pi^2 t^2 \Lambda_o^{-2} f(\eta),$$

where

$$f(\eta) = \left[\frac{\sin U(1+\eta^2)^{1/2}}{U(1+\eta^2)^{1/2}}\right]^2$$

and

$$U = \pi t\Lambda_o^{-1}.$$

When $t\Lambda_o^{-1}$ is very small, $f(\eta)$ tends asymptotically towards the function

$$f_1(\eta) = \left[\frac{\sin U\eta}{U\eta}\right]^2$$

and I_h towards the value given by geometrical theory. The condition for geometrical theory to apply is, therefore, that the crystal thickness be much smaller than the *Pendellösung* distance. In practice, the two theories agree to within a few per cent for a crystal

thickness smaller than or equal to a third of the *Pendellösung* distance [see Authier & Malgrange (1998)].

5.1.7. Intensity of plane waves in reflection geometry

5.1.7.1. *Thick crystals*

5.1.7.1.1. *Non-absorbing crystals*

Rocking curve. The geometrical construction in Fig. 5.1.3.5 shows that, in the Bragg case, the normal to the crystal surface drawn from the extremity of the incident wavevector intersects the dispersion surface either at two points of the same branch, P_1, P'_1, for branch 1, P_2, P'_2 for branch 2, or at imaginary points. It was shown in Section 5.1.2.6 that the propagation of the wavefields inside the crystal is along the normal to the dispersion surface at the corresponding tie points. Fig. 5.1.3.5 shows that this direction is oriented towards the outside of the crystal for tie points P'_1 and P'_2. In a very thick crystal, these wavefields cannot exist because there is always a small amount of absorption. One concludes that in the thick-crystal case and in reflection geometry, only one wavefield is excited inside the crystal. It corresponds to branch 1 on the low-angle side of the rocking curve and to branch 2 on the high-angle side. Using the same approximations as in Section 5.1.6.2, the amplitude $\mathbf{D}_{\mathbf{h}}^{(a)}$ of the wave reflected at the crystal surface is obtained by applying the boundary conditions, which are particularly simple in this case:

$$\mathbf{D_o} = \mathbf{D_o}^{(a)}, \ \mathbf{D_h}^{(a)} = \mathbf{D_h}.$$

The reflecting power is given by an expression similar to (5.1.6.7):

$$I_h = |\gamma||\xi_j|^2,$$

where the expression for ξ_j is given by (5.1.3.12), and $j = 1$ or 2 depending on which wavefield propagates towards the inside of the crystal. When the normal to the entrance surface intersects the dispersion surface at imaginary points, *i.e.* when $-1 < \eta < +1$,

$$|\xi|^2 = |\gamma|^{-1}, \ I_h = 1, \qquad (5.1.7.1)$$

and there is *total reflection*. Outside the total-reflection domain, the reflecting power is given by

$$I_h = \left[|\eta| - (\eta^2 - 1)^{1/2}\right]^2. \qquad (5.1.7.2)$$

The rocking curve has the well known top-hat shape (Fig. 5.1.7.1). Far from the total-reflection domain, the curve can be
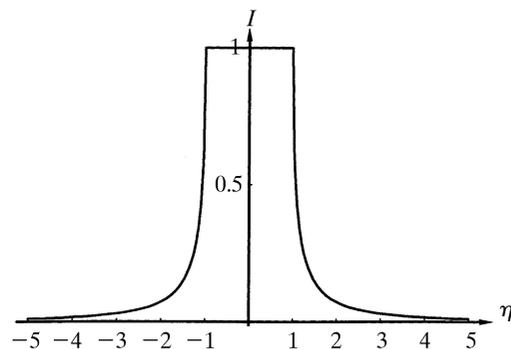

Fig. 5.1.7.1. Theoretical rocking curve in the reflection case for a non-absorbing thick crystal in terms of the deviation parameter.

approximated by the function

$$I_h \approx 1/(4\eta^2).$$

Width of the total-reflection domain. The width of the total-reflection domain is equal to $\Delta\eta = 2$ and its angular width is therefore equal, using (5.1.3.5), to 2δ, where δ is given by (5.1.3.6). It is proportional to the structure factor, the polarization factor C and the square root of the asymmetry factor $|\gamma|$. Using an asymmetric reflection, it is therefore possible to decrease the width at wish. This is used in monochromators to produce a pseudo plane wave [see, for instance, Kikuta & Kohra (1970)]. It is possible to deduce the value of the form factor from very accurate measurements of the rocking curve; see, for instance, Kikuta (1971).

Integrated intensity. The integrated intensity is defined by (5.1.6.8):

$$I_{hi} = 8\delta/3. \tag{5.1.7.3}$$

Penetration depth. Within the domain of total reflection, there are two wavefields propagating inside the crystal with imaginary wavevectors, one towards the inside of the crystal and the other one in the opposite direction, so that they cancel out and, globally, no energy penetrates the crystal. The absorption coefficient of the waves penetrating the crystal is

$$\mu = -4\pi K_{oi}\gamma_o = 2\pi\gamma_o(1 - \eta^2)^{1/2}/\Lambda_B, \tag{5.1.7.4}$$

where Λ_B is the value taken by Λ_o [equation (5.1.3.8)] in the Bragg case.

The penetration depth is a minimum at the middle of the reflection domain and at this point it is equal to $\Lambda_B/2\pi$. This attenuation effect is called *extinction*, and Λ_B is called the *extinction length*. It is a specific property owing to the existence of wavefields. The resulting propagation direction of energy is parallel to the crystal surface, but with a cross section equal to zero: it is an *evanescent wave* [see, for instance, Cowan *et al.* (1986)].

5.1.7.1.2. *Absorbing crystals*

Rocking curve. Since the sign of γ is negative, $[\eta^2 + S(\gamma h)]^{1/2}$ in (5.1.3.10) has a very large imaginary part when $|\eta_r| \leq 1$. It cannot be calculated using the same approximations as in the Laue case. Let us set

$$Z \exp(i\Psi') = \eta \mp (\eta^2 - 1)^{1/2}. \tag{5.1.7.5}$$

The reflecting power is

$$I_h = (F_h/F_{\bar{h}})^{1/2}Z^2, \tag{5.1.7.6}$$

where $Z = [L - (L^2 - 1)^{1/2}]^{1/2}, L = |\eta|^2 + \rho^2$ and $\rho = |\eta^2 - 1|$ is the modulus of expression (5.1.7.5) where the sign is chosen in such a way that Z is smaller than 1.

The expression for the reflected intensity in the absorbing Bragg case was first given by Prins (1930). The way of representing it given here was first used by Hirsch & Ramachandran (1950). The properties of the rocking curve have been described by Fingerland (1971).

There is no longer a total-reflection domain and energy penetrates the crystal at all incidence angles, although with a very high absorption coefficient within the domain $|\eta_r| \leq 1$. Fig. 5.1.7.2 gives an example of a rocking curve for a thick absorbing crystal. It was first observed by Renninger (1955). The shape is asymmetric and is due to the anomalous-absorption effect: it is lower than normal on the low-angle side, which is associated with wavefields belonging to branch 1 of the dispersion surface, and larger than normal on the high-angle side, which is associated with branch 2 wavefields. The amount of asymmetry depends on the value of the ratio A/B of the coefficients in the expression for the imaginary part
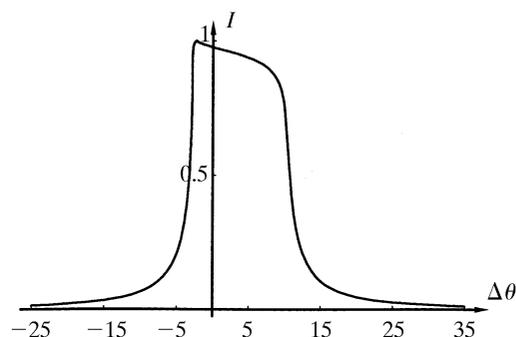

Fig. 5.1.7.2. Theoretical rocking curve in the reflection case for a thick absorbing crystal. The 400 reflection of GaAs using Cu $K\alpha$ radiation is shown.

of the deviation parameter in (5.1.3.7): the smaller this ratio, the more important the asymmetry.

Absorption coefficient. The effective absorption coefficient, taking into account both the Borrmann effect and extinction, is given by (Authier, 1986)

$$\mu = \mu_o + 2(|F_h F_{\bar{h}}|)^{1/2} \frac{R\lambda}{V(|\gamma|)^{1/2}} Z \sin(\beta + \Psi'),$$

where β is defined in equation (5.1.3.7) and Ψ' in equation (5.1.7.5), and where the sign is chosen in such a way that Z converges. Fig. 5.1.7.3 shows the variation of the penetration depth $z_o = \gamma_o/\mu$ with the deviation parameter.

5.1.7.2. *Thin crystals*

5.1.7.2.1. *Non-absorbing crystals*

Boundary conditions. If the crystal is thin, the wavefield created at the reflecting surface at A and penetrating inside can reach the back surface at B (Fig. 5.1.7.4a). The *incident* direction there points towards the *outside* of the crystal, while the *reflected* direction
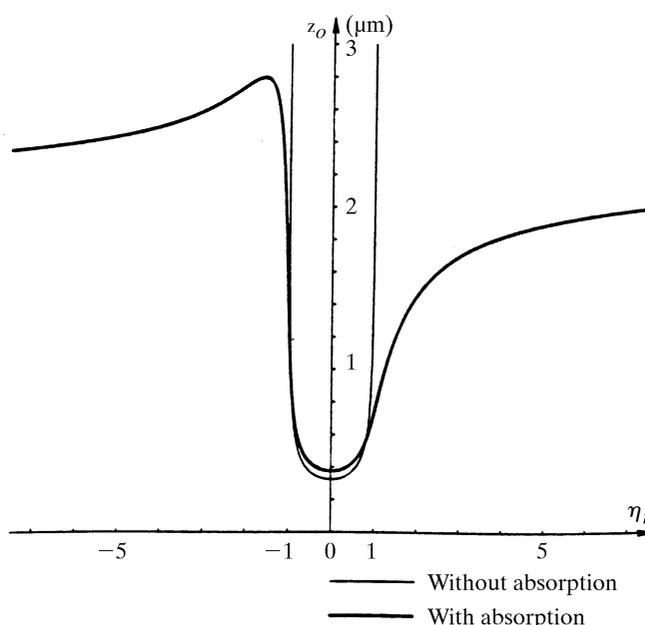

Fig. 5.1.7.3. Bragg case: thick crystals. Variation of the penetration depth with incidence angle (represented here by the dimensionless deviation parameter η). Thin curve: without absorption; thick curve: with absorption for the 400 reflection of GaAs using Cu $K\alpha$ radiation.
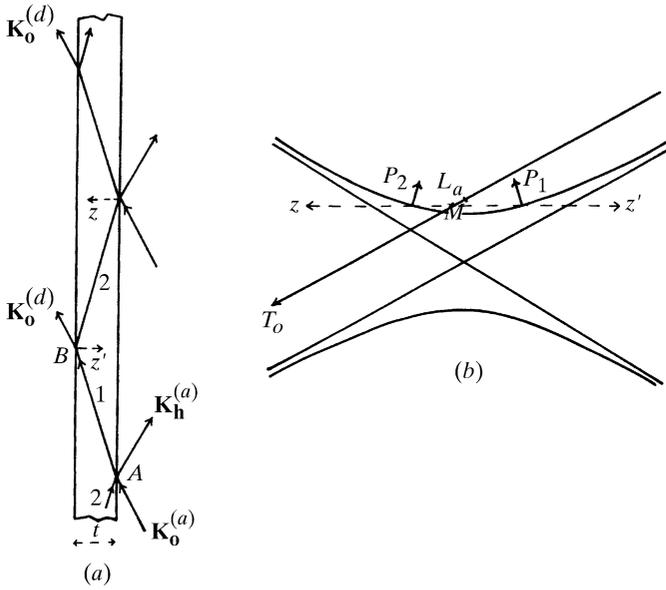
Fig. 5.1.7.4. Bragg case: thin crystals. Two wavefields propagate in the crystal. (*a*) Direct space; (*b*) reciprocal space.

points towards the inside. The wavefield propagating along AB will therefore generate at B:

(i) *a partially transmitted wave* outside the crystal, $\mathbf{D}_o^{(d)} \exp(-2\pi i \mathbf{K}_o^{(d)} \cdot \mathbf{r})$;

(ii) *a partially reflected wavefield* inside the crystal.

The corresponding tiepoints are obtained by applying the usual condition of the continuity of the tangential components of wavevectors (Fig. 5.1.7.4*b*). If the crystal is a plane-parallel slab, these points are M and P_2, respectively, and $\mathbf{K}_o^{(d)} = \mathbf{K}_o^{(a)}$.

The boundary conditions are then written:

(i) entrance surface:

$$D_{o1} + D_{o2} = D_o^{(a)}, \quad D_{h1} + D_{h2} = D_h^{(a)};$$

(ii) back surface:

$$D_{o1}\exp(-2\pi i\mathbf{K}_{\mathbf{o}1}\cdot\mathbf{r}) + D_{o2}\exp(-2\pi i\mathbf{K}_{\mathbf{o}2}\cdot\mathbf{r}) = D_o^{(a)}\exp\left(-2\pi i\mathbf{K}_{\mathbf{o}}^{(d)}\cdot\mathbf{r}\right),$$
$$D_{h1}\exp(-2\pi i\mathbf{K}_{\mathbf{h}1}\cdot\mathbf{r}) + D_{h2}\exp(-2\pi i\mathbf{K}_{\mathbf{h}2}\cdot\mathbf{r}) = 0.$$

Rocking curve. Using (5.1.3.10), it can be shown that the expressions for the intensities reflected at the entrance surface and transmitted at the back surface, I_h and I_o, respectively, are given by different expressions within total reflection and outside it:

(i) $|\eta| < 1$:

$$I_h = |\gamma|\frac{|D_h^{(a)}|^2}{|D_o^{(a)}|^2} = \frac{\cosh^2[\pi(t/\Lambda_B)(1-\eta^2)^{1/2}] - 1}{\cosh^2[\pi(t/\Lambda_B)(1-\eta^2)^{1/2}] - \eta^2}$$
$$I_o = \frac{|D_o^{(d)}|^2}{|D_o^{(a)}|^2} = \frac{1 - \eta^2}{\cosh^2[\pi(t/\Lambda_B)(1-\eta^2)^{1/2}] - \eta^2},$$

(5.1.7.7*a*)

where Λ_B is the value taken by Λ_o [equation (5.1.3.8)] in the Bragg case.

There is no longer a total-reflection domain but the extinction effect still exists, as is shown by the hyperbolic cosine term. The maximum height of the rocking curve decreases as the thickness of the crystal decreases.

(ii) $|\eta| > 1$:

$$I_h = \frac{1 - \cos^2[\pi(t/\Lambda_B)(\eta^2-1)^{1/2}]}{\eta^2 - \cos^2[\pi(t/\Lambda_B)(\eta^2-1)^{1/2}]},$$
$$I_o = \frac{\eta^2 - 1}{\eta^2 - \cos^2[\pi(t/\Lambda_B)(\eta^2-1)^{1/2}]}.$$

(5.1.7.7*b*)

The cosine terms show that the two wavefields propagating within the crystal interfere, giving rise to *Pendellösung* fringes in the rocking curve. These fringes were observed for the first time by Batterman & Hildebrandt (1967, 1968). The angular positions of the minima of the reflected beam are given by

$$\eta = \mp(K^2\Lambda_B^2 t^{-2} + 1)^{1/2},$$

where K is an integer.

Integrated intensity. The integrated intensity is

$$I_{hi} = \pi\delta\tanh[\pi t/\Lambda_B], \qquad (5.1.7.8)$$

where t is the crystal thickness. When this thickness becomes very large, the integrated intensity tends towards

$$I_{hi} = \pi\delta. \qquad (5.1.7.9)$$

This expression differs from (5.1.7.3) by the factor π, which appears here in place of 8/3. von Laue (1960) pointed out that because of the differences between the two expressions for the reflecting power, (5.1.7.2) and (5.1.7.7*b*), perfect agreement could not be expected. Since some absorption is always present, expression (5.1.7.3), which includes the factor 8/3, should be used for very thick crystals. In the presence of absorption, however, expression (5.1.7.8) for the reflected intensity for thin crystals does tend towards that for thick crystals as the crystal thickness increases.

Comparison with geometrical theory. When t/Λ_B is very small (thin crystals or weak reflections), (5.1.7.8) tends towards

$$I_{hi} = R^2\lambda^2 t|F_h|^2/(V^2\gamma_o\sin 2\theta), \qquad (5.1.7.10)$$

which is the expression given by geometrical theory. If we call this intensity I_{hi}(geom.), comparison of expressions (5.1.7.8) and (5.1.7.10) shows that the integrated intensity for crystals of intermediate thickness can be written

$$I_{hi} = I_{hi}(\text{geom.})\frac{\tanh(\pi t/\Lambda_B)}{(\pi t/\Lambda_B)}, \qquad (5.1.7.11)$$

which is the expression given by Darwin (1922) for primary extinction.

5.1.7.2.2. *Absorbing crystals*

Reflected intensity. The intensity of the reflected wave for a thin absorbing crystal is

$$I_h = |\gamma|\left|\frac{D_h^{(a)}}{D_o^{(a)}}\right|^2$$
$$= \left|\frac{F_h}{F_{\bar{h}}}\right|\frac{\cosh 2b - \cos 2a}{L\cosh 2b + (L^2-1)^{1/2}\sinh 2b - \cos(2a+2\Psi')},$$

(5.1.7.12)

where

$$2a = [\pi t/\Lambda_B]\rho\cos(\beta+\omega),$$
$$2b = [\pi t/\Lambda_B]\rho\sin(\beta+\omega).$$

547

L, ρ and ψ' are defined in (5.1.7.5), β is defined in (5.1.3.7) and ω is the phase angle of $(\eta^2 - 1)^{1/2}$.

Comparison with geometrical theory. When t/Λ_B decreases towards zero, expression (5.1.7.12) tends towards $[\sin(\pi t \eta/\Lambda_B)/\eta]^2$; using (5.1.3.5) and (5.1.3.8), it can be shown that expression (5.1.7.12) can be written, in the non-absorbing symmetric case, as

$$I_h = \frac{R^2 \lambda^2 C^2 |F_h|^2 t^2}{V^2 \sin^2 \theta} \left\{ \frac{\sin[2\pi k \cos(\theta) t \Delta\theta]}{[2\pi k \cos(\theta) t \Delta\theta]} \right\}^2, \qquad (5.1.7.13)$$

where d is the lattice spacing and $\Delta\theta$ is the difference between the angle of incidence and the middle of the reflection domain. This expression is the classical expression given by geometrical theory [see, for instance, James (1950)].

5.1.8. Real waves

5.1.8.1. *Introduction*

The preceding sections have dealt with the diffraction of a plane wave by a semi-infinite perfect crystal. This situation is actually never encountered in practice, although with various devices, in particular using synchrotron radiation, it is possible to produce highly collimated monochromated waves which behave like pseudo plane waves. The wave from an X-ray tube is best represented by a spherical wave. The first experimental proof of this fact is due to Kato & Lang (1959) in the transmission case. Kato extended the dynamical theory to spherical waves for non-absorbing (1961*a,b*) and absorbing crystals (1968*a,b*). He expanded the incident spherical wave into plane waves by a Fourier transform, applied plane-wave dynamical theory to each of these components and took the Fourier transform of the result again in order to obtain the final solution. Another method for treating the problem was used by Takagi (1962, 1969), who solved the propagation equation in a medium where the lateral extension of the incident wave is limited and where the wave amplitudes depend on the lateral coordinates. He showed that in this case the set of fundamental linear equations (5.1.2.20) should be replaced by a set of partial differential equations. This treatment can be applied equally well to a perfect or to an imperfect crystal. In the case of a perfect crystal, Takagi showed that these equations have an analytical solution that is identical with Kato's result. Uragami (1969, 1970) observed the spherical wave in the Bragg (reflection) case, interpreting the observed intensity distribution using Takagi's theory. Saka *et al.* (1973) subsequently extended Kato's theory to the Bragg case.

Without using any mathematical treatment, it is possible to make some elementary remarks by considering the fact that the divergence of the incident beam falling on the crystal from the source is much larger than the angular width of the reflection domain. Fig. 5.1.8.1(*a*) shows a spatially collimated beam falling on a crystal in the transmission case and Fig. 5.1.8.1(*b*) represents the corresponding situation in reciprocal space. Since the divergence of the incident beam is larger than the angular width of the dispersion surface, the plane waves of its Fourier expansion will excite every point of both branches of the dispersion surface. The propagation directions of the corresponding wavefields will cover the angular range between those of the incident and reflected beams (Fig. 5.1.8.1*a*) and fill what is called the *Borrmann triangle*. The intensity distribution within this triangle has interesting properties, as described in the next two sections.

5.1.8.2. *Borrmann triangle*

The first property of the Borrmann triangle is that the angular density of the wavefield paths is inversely proportional to the
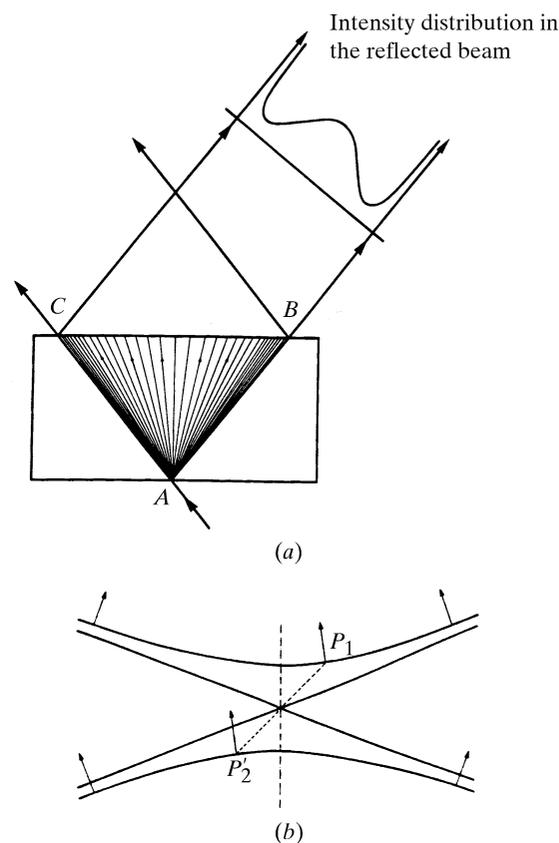

Fig. 5.1.8.1. Borrmann triangle. When the incident beam is divergent, the whole dispersion surface is excited and the wavefields excited inside the crystal propagate within a triangle filling all the space between the incident direction, *AC*, and the reflected direction, *AB*. Along any direction *Ap* within this triangle two wavefields propagate, having as tie points two conjugate points, *P* and *P'*, at the extremities of a diameter of the dispersion surface. (*a*) Direct space; (*b*) reciprocal space.

curvature of the dispersion surface around their tie points. Let us consider an incident wavepacket of angular width $\delta(\Delta\theta)$. It will generate a packet of wavefields propagating within the Borrmann triangle. The angular width $\Delta\alpha$ (Fig. 5.1.8.2) between the paths of the corresponding wavefields is related to the radius of curvature $\mathcal{R}$ of the dispersion surface by

$$\mathcal{A} = \Delta\alpha/\delta(\Delta\theta) = k \cos\theta(\mathcal{R}\cos\alpha), \qquad (5.1.8.1)$$

where α is the angle between the wavefield path and the lattice planes [equation (5.1.2.26)] and $\mathcal{A}$ is called the amplification ratio. In the middle of the reflecting domain, the radius of curvature of the dispersion surface is very much shorter than its value, k, far from it (about 10^4 times shorter) and the amplification ratio is therefore very large. As a consequence, the energy of a wavepacket of width $\delta(\Delta\theta)$ in reciprocal space is spread in direct space over an angle $\Delta\alpha$ given by (5.1.8.1). The intensity distribution on the exit surface *BC* (Fig. 5.1.8.1*a*) is therefore proportional to $I_h/\mathcal{A}$. It is represented in Fig. 5.1.8.3 for several values of the absorption coefficient:

(i) Small values of $\mu_o t$ (less than 2 or 3) (Fig. 5.1.8.3*a*). The intensity distribution presents a wide minimum in the centre where the density of wavefields is small and increases very sharply at the edges where the density of wavefields is large, although it is the reverse for the reflecting power I_{hj}. This effect, called the *margin effect*, was predicted qualitatively by Borrmann (1959) and von Laue (1960), demonstrated experimentally by Kato & Lang (1959), and calculated by Kato (1960).